A metastable rRNA junction essential for bacterial 30S biogenesis

Indra Mani Sharma[1],[†], Mollie C. Rappé[1],[†], Balasubrahmanyam Addepalli[2], Wade W. Grabow[3], Zhuoyun Zhuang[3], Sanjaya C. Abeysirigunawardena[1], Patrick A. Limbach[2], Luc Jaeger[3],[*] and Sarah A. Woodson[1],[*]

[1]T. C. Jenkins Department of Biophysics, Johns Hopkins University, 3400 N. Charles St., Baltimore, MD 21218, USA, [2]Department of Chemistry, Rieveschl Laboratories for Mass Spectrometry, University of Cincinnati, Cincinnati, OH 45221, USA and [3]Department of Chemistry and Biochemistry, University of California, Santa Barbara, CA 93106-9510, USA

ABSTRACT

Tertiary sequence motifs encode interactions between RNA helices that create the three-dimensional structures of ribosomal subunits. A Right Angle motif at the junction between 16S helices 5 and 6 (J5/6) is universally conserved amongst small subunit rRNAs and forms a stable right angle in minimal RNAs. J5/6 does not form a right angle in the mature ribosome, suggesting that this motif encodes a metastable structure needed for ribosome biogenesis. In this study, J5/6 mutations block 30S ribosome assembly and 16S maturation in *Escherichia coli*. Folding assays and in-cell X-ray footprinting showed that J5/6 mutations favor an assembly intermediate of the 16S 5′ domain and prevent formation of the central pseudoknot. Quantitative mass spectrometry revealed that mutant pre-30S ribosomes lack protein uS12 and are depleted in proteins uS5 and uS2. Together, these results show that impaired folding of the J5/6 right angle prevents the establishment of inter-domain interactions, resulting in global collapse of the 30S structure observed in electron micrographs of mutant pre-30S ribosomes. We propose that the J5/6 motif is part of a spine of RNA helices that switch conformation at distinct stages of assembly, linking peripheral domains with the 30S active site to ensure the integrity of 30S biogenesis.

INTRODUCTION

The core of the ribosome is largely composed of rRNA (1,2) and adopts a similar three-dimensional structure in ribosomes from all kingdoms of life (3). Conserved sequence motifs in the rRNA encode for tertiary structural motifs (or modules) that contribute to the formation of the tertiary architecture of the ribosome and create the active sites for tRNA binding and peptide synthesis (4–7). Although most RNA tertiary motifs are needed to stabilize the mature structure of the ribosome, some motifs may exchange interaction partners or refold during the assembly process. An outstanding question is how RNA motifs in disparate regions of the ribosome communicate with each other to ensure complete assembly.

The Right Angle (RA) is a complex RNA sequence motif identified at several locations in small subunit (SSU) and large subunit (LSU) rRNAs (Supplementary Figure S1) (8–10). The RA motif comprises an along-groove stacking interaction between neighboring helices (11) that is stabilized by two GA-minor motifs (Figure 1A, left panel, Supplementary Figure S2). The RA sequence at the junction (J) of helix (h) 5 and h6 (J5/6) in the SSU rRNA is universally conserved (Supplementary Figure S1). Surprisingly, J5/6 does not form a Right Angle in mature ribosomes (Figures 1A, right panel and 1B, inset, Supplementary Figure S2A). Instead, the tip of h15 interacts with the along-groove stacking surface of h5, forcing h6 into the splayed (obtuse) angle that defines the spur of the small subunit of the ribosome (Figure 1B, Supplementary Figure S2B).

Earlier footprinting data suggested that J5/6 in the 16S 5′ domain undergoes specific conformational changes during

*To whom correspondence should be addressed. Tel: +1 410 516 2015; Fax: +1 410 516 4118; Email: swoodson@jhu.edu
Correspondence may also be addressed to Luc Jaeger. Tel: +1 805 893 3628; Fax: +1 805 893 4120; Email: jaeger@chem.ucsb.edu
†These authors contributed equally to the paper as first authors.
Present addresses:
Mollie C. Rappé, Sandia National Laboratory, Sandia, NM 87185, USA.
Sanjaya C. Abeysirigunawardena, Department of Chemistry and Biochemistry, Kent State University, Kent, OH 44242, USA.
Wade W. Grabow, Department of Chemistry and Biochemistry, Seattle Pacific University, 3307 Third Avenue West, Seattle, WA 98119, USA.
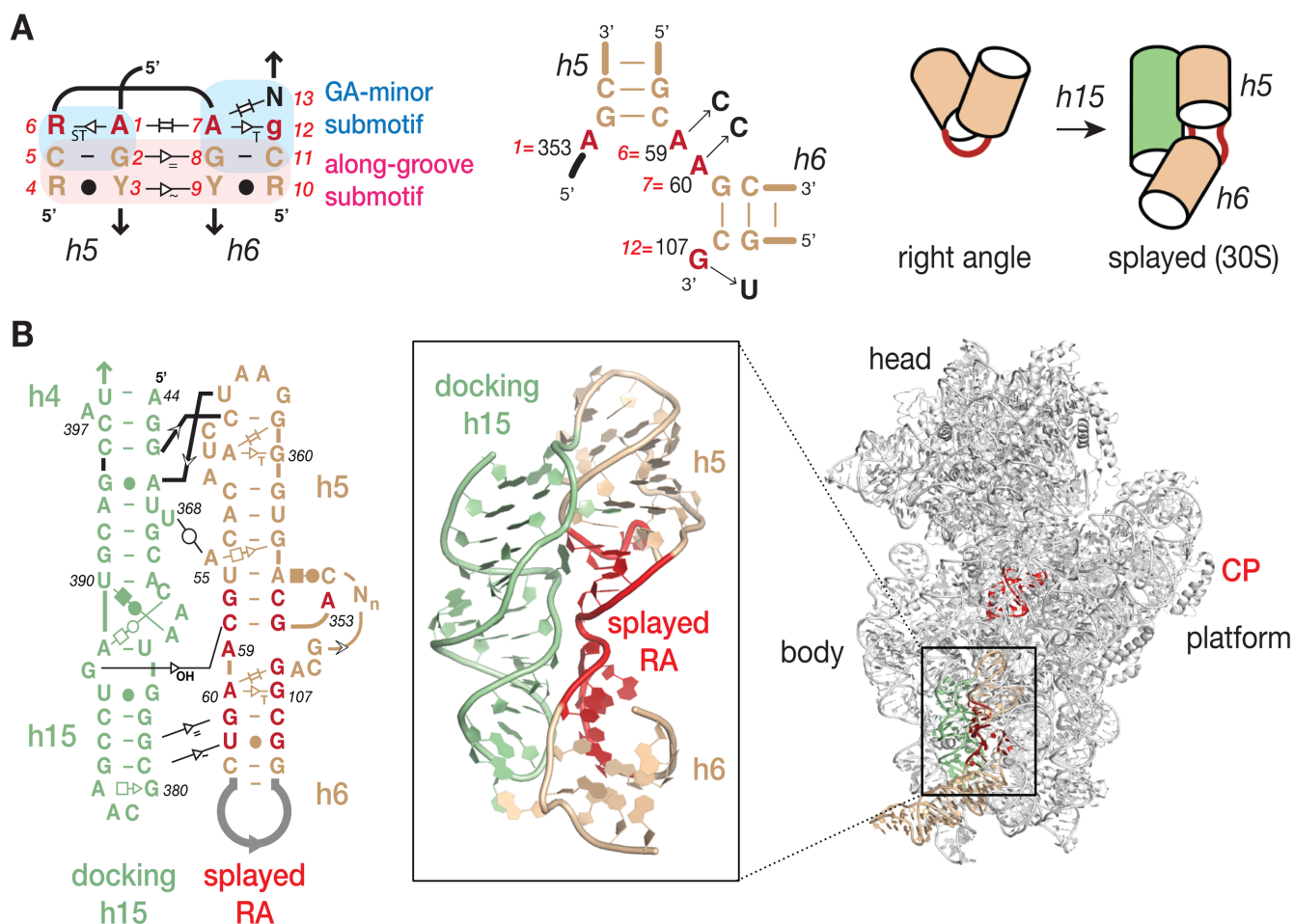
Figure 1. An essential helix junction motif in the 16S rRNA. (**A**) Consensus sequence for the Right Angle (RA) motif (9) comprised of the Along-Groove stacking submotif (pink box) and two GA-minor submotifs (blue boxes). The RA motif between 16S h5 and h6 (J5/6) is destabilized by mutations used in this study at positions 1, 6, 7 and 12 (see also Figure 2B). Helices 5 and 6 form a right angle in isolation but are splayed apart to interact with h15 in the 30S ribosome. (**B**) Secondary and tertiary interactions between the J5/6 RA motif (h5, h6 in wheat; J5/6 RA motif in red) and its docking helix (h15 in pale green) in the three-dimensional structure of 30S ribosome (2I2P; (56)). The central pseudoknot (CP) is in bright red. Symbols and abbreviations: R, purine; Y, pyrimidine; N, any nucleotide. For base pair symbols, see legend of Supplementary Figure S2: Watson–Crick (WC), Hoogsteen (HG), and shallow groove (SG) edges are indicated by circles, squares and triangles, respectively.

30S assembly. It is one of the slowest regions of the 16S 5′ domain to fold in 20 mM Mg^{2+}, indicating that proteins are needed to guide this region of the rRNA to its final structure (12). Residues in h6 are buried when the RNA is folded in ≤2.5 mM $MgCl_2$, while higher $MgCl_2$ or ribosomal proteins are needed to bury h15, suggesting that h6 packs with other helices before it interacts with h15 (Supplementary Figure S2B). Tethered Fe(II) hydroxyl radical cleavage of rRNA residues near the N-terminal alpha helix of bS20, which lies on one side of J5/6, revealed different intermediate structures in the presence of protein bS20 or bS20 plus uS17, compared with the mature 30S ribosome (13). Protein bS16, which interacts with 16S h15 on the other side of J5/6, holds h15 against h6 when h6 is in its proper orientation and produces a footprinting pattern similar to that in the complete 30S ribosome (13–15). Importantly, protein bS20, which contacts J5/6, switches the 16S rRNA to a structure that is able to productively add protein bS16 (16), both increasing the probability of bS16 binding and the lifetime of bS16 complexes (17).

J5/6 is structurally coupled to a second conformational switch at 16S h3, which is coincidently joined to h18 through another RA motif (9). Hydroxyl radical footprinting and single molecule (sm)FRET showed that the 16S 5′ domain passes through an assembly intermediate in which 16S h3 is flipped out of the structure rather than docked against protein uS4, as it is in the mature 30S ribosome (15,18). Binding of protein bS16 greatly favors h3 docking, which in turn connects the 5′ domain to the central and 3′ domains via the central pseudoknot (14,15,19). Thus, J5/6 participates in a chain of RNA and protein interactions that connect h6 (30S spur) with the central pseudoknot of the 30S ribosome (Figures 1B and 8).

This evidence that the RNA helices around h5 and h6 change conformation during 30S assembly, and the conservation of the J5/6 RA motif among SSU rRNAs, motivated us to inquire whether this motif is required for ribosome assembly. Here, we show that mutations in J5/6 block 30S maturation and impair formation of the central pseudoknot, resulting in a total collapse of interactions between

the major 30S domains. The results demonstrate that RNA motifs far from the active site of the ribosome are functionally important and may encode metastable conformations that are needed at specific stages of assembly, thus accounting for their conservation during molecular evolution.

MATERIALS AND METHODS

TectoRNA design, synthesis and assembly

The tectoRNA system (Supplementary Table S1) used in the study was designed as previously reported (9). The equilibrium constant of dissociation (K_d) of transcribed tectoR-NAs was measured by mixing equimolar amounts of each tectoRNA at various concentrations (typically 10 nM to 20 μM) in water. Samples were denatured 2 min at 95°C, snap-cooled 3 min at 4°C, and incubated 20 min at 30°C in association buffer [89 mM Tris–borate pH 8.2, 50 mM KCl and 15 mM Mg(OAc)$_2$]. The probe (containing the GGAA tetraloop and 11-nt receptor) contained a fixed amount of 3′-[^{32}P]-pCp-labeled RNA (~1 nM final). Samples were cooled on ice before addition of blue loading buffer (magnesium buffer, 0.01% bromophenol blue, 0.01% xylene cyanol, 50% glycerol). tectoRNA assembly was monitored by native 10% (29:1) PAGE at a maximum temperature of 10°C for 3 h in [89 mM Tris–borate, pH 8.3, and 15 mM Mg(OAc)$_2$].

K_d values were derived from the titration experiments performed at 10°C (Supplementary Table S2). Monomers [Probe (P_{h15}) and RA attenuator constructs ($M_{J5/6}$)] and heterodimers [$P_{h15} \times M_{J5/6}$] were quantified using Image-Quant. K_d values for the equilibrium reaction $P_{h15} + M_{J5/6} \rightarrow P_{h15} \times M_{J5/6}$ were determined using a non-linear fit of the experimental data to the equation: $f = [2\beta M_0 + K_d - (4M_0\beta K_d + K_d^2)^{0.5}]/2M_0$, where f is the fraction of the RNA heterodimer, defined as the ratio of the dimer ($P_{h15} \times M_{J5/6}$) to the total RNA species ($P_{h15} + M_{J5/6} + P \times M_{J5/6}$), M_0 is the total concentration of the probe, and β is the maximum fraction of RNA able to dimerize (20). In the case where β is equal to 1, the equation simplifies to $K_d = [(M_0)(1 - f)^2]/f$ so that $M_0/2$ represents the value at which 50% of the heterodimer is formed. Each reported K_d represents the average of a minimum of three independent experiments.

Bacterial strains and plasmids

Bacterial strains, plasmids, primers and oligonucleotides used in the study are listed in Supplementary Tables S3–S5. The J5/6 mutations were introduced into pLK45 expressing the *Escherichia coli rrnB* operon from λ pL (21,22), and into pSpur, a pLK45 derivative with an MS2-hairpin at the tip of helix 6 (23).

Bacterial growth assays

For plating assays, DH1/pCI^{857} cells with pLK45 derivatives containing J5/6 mutations were grown in LB containing 25 μg/ml kanamycin and 25 μg/ml carbenicillin at 30°C until mid-log (OD$_{600}$ = 0.45–0.6). The cultures were diluted to OD = 0.05 and 5 μl of eight serial 10-fold dilutions was spotted onto LB agar containing 25 μg/ml kanamycin and 25 μg/ml carbenicillin or 25

μg/ml carbenicillin and 10 μg/ml spectinomycin. Plates were incubated at 32°C (repressive) or 42°C (permissive) as previously described (22). For growth in liquid media, $\Delta 7rrn$/pTRNA67/pHK-*rrnC$^+$ sacB* cells (24,25) transformed with pLK45 or pLK45-Triple were grown at 37°C in LB (100 μg/ml ampicillin and 50 μg/ml kanamycin or 100 μg/ml ampicillin only). After 120 min, 3% sucrose was added to the ampicillin-only cultures to select for loss of pHK-*rrnC$^+$ sacB*. The cell density (OD$_{600}$) was recorded every 30 min.

Analytical sucrose gradients and primer extension

Analytical 10–40% sucrose gradients (20 mM Tris–HCl pH 7.8, 10 mM MgCl$_2$, 100 mM NH$_4$Cl, 2 mM DTT) were performed as previously described (26). Gradients were analyzed with a BioComp piston fractionator, and UV absorbance traces at 254 nm were recorded with WINDAQ software (DataQ). Fractions (400 μl) from peaks of interest were precipitated with ethanol overnight, extracted four times with phenol, twice with chloroform, and precipitated with ethanol prior to primer extension analysis. To map the 16S 5′ ends by primer extension, either 2 μg total RNA or 500 ng purified 16S rRNA (1 pmol) was annealed to 1 pmol ^{32}P-labeled primer **161** (Supplementary Table S4) and extended by SuperScript III reverse transcriptase (Invitrogen) at 52.5°C for 30 min (14,27). Samples were analyzed by denaturing 8% PAGE. For total RNA from pSpur-transformed cells, the counts in the major cDNA products corresponding to chromosomally-derived 16S and 17S rRNA and plasmid-derived MS2–16S and MS2–17S rRNA were normalized to the total amount of mature (16S) rRNA, as *E. coli* regulates rRNA expression levels to control for gene dosage (28,29).

SHAPE chemical probing and ensemble FRET of 16S 5′ domain complexes

SHAPE experiments were performed *in vitro* on the 16S 5′ domain RNA (with a 3′ 1199 extension), with or without J5/6 mutations, and with or without proteins uS4, bS16, uS17, and bS20), as described previously (17,30) and in Supplementary Methods. Ensemble FRET experiments were performed in 80 mM K-Hepes pH 7.5, 330 mM KCl, 20 mM MgCl$_2$ at 37°C as previously described (19).

In vivo X-ray footprinting

MRE600 (RNase I$^-$) cells transformed with pSpur and pSpur J5/6 derivatives were grown in LB at 37°C to mid-log (OD$_{600}$ 0.4–0.6), frozen in 5 μl samples, and exposed for 25–100 ms to a synchrotron X-ray beam in a pre-chilled multi-sample holder on a motorized stage (X28C, National Synchrotron Light Source at Brookhaven National Laboratory) (31). Cell pellets were resuspended in 500 μl RNAprotect bacteria reagent (Qiagen) and total RNA extracted (RNeasy mini prep, Qiagen). The cleavage pattern was assayed by extension of a ^{32}P-labeled Spc^R allele specific primer (Supplementary Table S4). Dideoxynucleotide sequencing ladders were generated on un-irradiated RNA templates. Gels were quantified using SAFA (32) and normalized to a strong band with minimal variation between

lanes. After normalization, the nucleotide intensities for the three technical replicates were averaged. The error bars indicate the standard deviation of the triplicates. For a few nucleotides (<5%), the band intensity of one replicate was quite different from the other two, and such outliers were discarded.

Quantitative mass spectrometry of MS2-tagged ribosomes

Affinity purification of pSpur-WT or pSpur-Triple ribosomes was carried out as previously described (23,33) with modifications described in Supplemental Methods. Purified ribosomal protein (∼3 μg) was digested with trypsin (0.30 μg) (34) before LC-MS/MS analysis on an Orbitrap Fusion Lumos™ mass spectrometer equipped with an electrospray ionization (ESI) source (see Supplemental Methods for details). The Orbitrap raw mass spectral data files were analyzed and matched by Thermo Proteome Discoverer (version 2.1) featuring the SEQUEST™ protein search algorithm and annotated *E. coli* proteome database for protein identification.

Accessibility of central pseudoknot

Oligonucleotide-directed RNase H cleavage of residues in the central pseudoknot was performed as previously described (35) using DNA oligomers anti-CP and anti-h21 (Supplementary Table S4) that base pair with 16S rRNA regions 906–920 and 589–603, respectively. MS2-tagged wild type and triple mutant complexes were purified by affinity as described in Supplemental Methods. pSpur-WT ribosomes were split at low MgCl$_2$ and the 30S complex repurified from a sucrose gradient before hybridization with anti-sense oligonucleotide. pSpur-Triple complexes were used without further purification. RNase H reactions were performed in 20 mM Tris–HCl pH7.5, 10 mM MgCl$_2$, 40 mM NH$_4$Cl, 60 mM KCl, 3 mM DTT with 3 or 33 μM oligomer, 50 nM 30S and 5 U RNase H on ice for 16 hrs. The cleavage products were resolved on a 2% agarose gel and stained with ethidium bromide.

Negative stain electron microscopy

WT and triple mutant 30S ribosome samples were imaged by negative stain transmission electron microscopy (36), as described in Supplemental Methods. Particles resembling 30S complexes were counted manually (>100 for WT and >50 for triple mutant 30S).

RESULTS

16S J5/6 junction forms a stable right angle

We confirmed that the h5 and h6 region of the *Escherichia coli* 16S rRNA folds into a right angle, using a minimal tectoRNA folding model described previously (9). TectoRNAs contain specific RNA structural modules that can control self-assembly into predefined, larger structures (37–40). In this assay (9), the RA conformation of the J5/6 test RNA attenuates its association with a second probe RNA that mimics 16S h15 (Figure 2A). The binding equilibrium between the test and probe tectoRNAs allows the relative stability of

the RA conformation, $\Delta\Delta G_{AT}$, to be determined from the degree of attenuation. We used this system to test the stability of the RA motif in 26 natural and synthetic variations of the GA minor submotifs (Figure 2B). The free energies obtained from the binding experiments showed that the J5/6 junction from *E. coli* 16S rRNA forms a particularly stable RA structure ('AAAG' in Figure 2C), compared to the other variants tested. Moreover, those variants that are the most prevalent among bacterial and eukaryotic SSU RNAs typically formed a stable RA structure in the tectoRNA system (blue and green bars; Figure 2C). By contrast, synthetic sequences designed to disrupt the GA minor motifs or alter the inter-helix stacking were 1.2–2.2 kcal/mol less stable than the *E. coli* 16S J5/6 motif (orange bars; Figure 2C).

Mutations in 16S J5/6 junction are recessive lethal in E. coli

To study the importance of the J5/6 motif for 30S ribosome biogenesis, we designed mutations in *E. coli* 16S J5/6 (Figure 1A, middle panel) that were intended to destabilize the right angle between h5 and h6, without destabilizing tertiary interactions between J5/6 and h15 in the mature ribosome (Figure 1B, middle panel). The chosen mutations – G107U (single), A59, 60C (Double), and A59, 60C, G107U (Triple) correspond to positions 12, 6, 7 of the RA motif (Figure 1A), and were found to destabilize the right angle conformation in experiments with minimal tectoRNAs, as predicted (Figure 2C).

These single, double or triple J5/6 mutations were introduced into pLK45, which expresses the *rrnB* operon from the λ pL promoter under the control of a temperature-sensitive λ repressor (cI^{857}) (21,22). pLK45 also contains a 16S mutation that makes 30S ribosomes containing plasmid-encoded rRNA resistant to spectinomycin (spc^R). *E. coli* cells (DH1/pCI^{857}) containing plasmids with J5/6 mutations grew nearly as well as cells containing the parental (WT J5/6) pLK45 at 42°C in the absence of spectinomycin (Figure 3A, top panel). By contrast, cells expressing the J5/6 mutations were unable to grow in the presence of spectinomycin, indicating that ribosomes containing mutant 16S rRNA were not functional (Figure 3A, bottom panel).

To further test whether strains bearing J5/6 mutations are viable, J5/6 WT and J5/6 triple mutant pLK45 plasmids were transformed into an *E. coli* strain that lacks all seven chromosomal rRNA operons and contains a sucrose-sensitive plasmid expressing the *rrnC* operon (Δ7*rrn*/pTRNA67/pHK-*rrnC*$^+$*sacB*) (24,25). In the presence of the *rrnC*$^+$*sacB* helper plasmid, both strains were able to grow at 37°C (Figure 3B, solid lines). Upon selecting for the loss of the pHK-*rrnC*$^+$*sacB* helper plasmid with sucrose, the cells transformed with WT J5/6 pLK45 recovered after a few generations. By contrast, cells transformed with mutant J5/6 pLK45 derivatives did not recover growth (Figure 3B, dotted lines). Thus, both assays showed that 30S ribosomes containing mutations in the J5/6 right angle motif do not support cell growth.

J5/6 mutant ribosomes cannot mature

To examine if the J5/6 mutants cannot support growth because of a defect in 30S assembly, the J5/6 mutations were
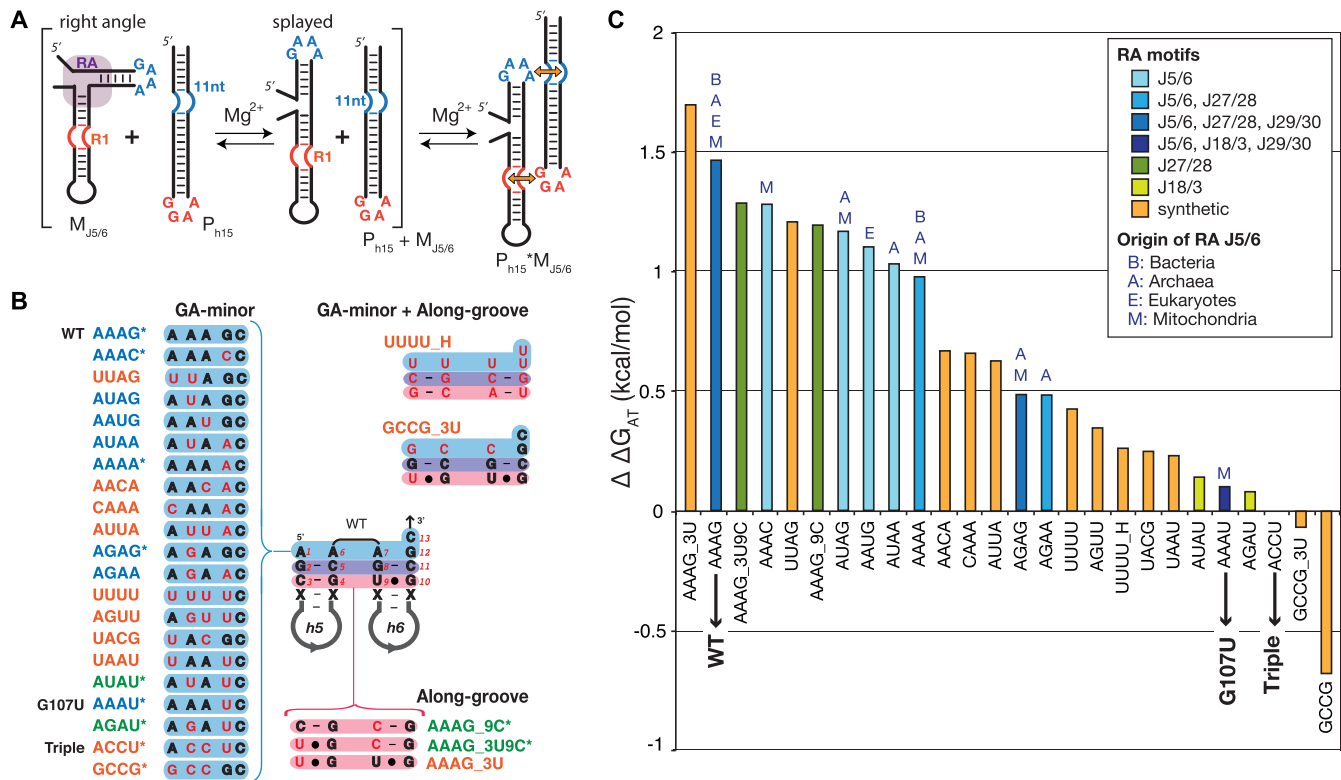
Figure 2. Thermodynamics of minimal RA folding using tectoRNA assembly. (**A**) Schematic of the experimental strategy: each RNA mimic of 16S J5/6 ($M_{J5/6}$) contains an RA sequence variant (purple box) at the junction between a hairpin containing a GAAA tetraloop (blue) and a second hairpin with a GGAA R1 receptor (red). $M_{J5/6}$ molecules are evaluated for their ability to bind to a probe that mimics 16S h15 (P_{h15}) and that also contains a GAAA 11-nt receptor (blue) and a GGAA tetraloop (red). $M_{J5/6}$ can only dock with P_{h15} by adopting the splayed conformation. (**B**) List of J5/6 variants tested in the tectoRNA system. The WT J5/6 sequence (AAAG) is used as a reference and sequence variations are indicated in red. Construct variants are named after GA-minor positions 1_6_7_12 (in blue) as well as sequence variations (in red) in the along groove submotif (in pink). Asterisks indicate constructs previously tested (9). (**C**) Apparent free energy of attenuation of tectoRNA assembly at 10°C: $\Delta\Delta G_{AT} = \Delta G^{J5/6} - \Delta G^{ref}$, where $\Delta G^{J5/6}$ is the free energy of $M_{J5/6}$ and P_{h15} dimerization and ΔG^{ref} is the same for the $M_{J5/6}$ reference RNA, which was chosen to be the triple mutant ACCU. The letters below each column refer to the sequence variants in (B). The column color indicates whether the RA sequence motif is natural (J5/6, blue; other rRNA, green) or synthetic (orange). For J5/6 RA sequences, letters indicate the phyletic origin, as in the key.

introduced into pSpur, a pLK45 derivative with an MS2-hairpin at the tip of helix 6 (23). The 36 nt MS2 tag allowed the expression and maturation of the plasmid-encoded 16S rRNA to be followed by primer extension against a background of chromosomally-encoded 30S subunits (Figure 3C). A polysome profile from MRE600/pSpur (WT J5/6) cells showed a pronounced 70S peak, smaller 30S and 50S peaks, and detectible 2X and 3X polyribosome peaks (Figure 3D, left panel). Primer extension analysis of 5′ end processing of the 16S rRNA revealed 75% immature rRNA in the lightest fraction of the 30S peak and a tiny fraction of immature rRNA in the 70S peak, as expected (Figure 3E, left panel). Compared to the chromosomally-encoded 16S rRNA, a higher proportion of plasmid-derived MS2–16S rRNA was found in the 30S peak fractions than the 70S peak fractions. The MS2-tagged rRNA was processed normally, however, and able to form 70S ribosomes, as observed previously (23).

By contrast, MRE600/pSpur-Triple mutant cells contained more free 30S and 50S subunits as well as smaller 2X and 3X polyribosome peaks (Figure 3D, right panel). In addition, the 30S peak was substantially shifted toward lighter (21S – 26S) fractions, indicating a defect in 30S ribo-

some assembly and a build-up of immature pre-30S particles. This was confirmed by primer extension analysis (Figure 3E, right panel), which showed that the 21–26S and 30S fractions mostly contained immature MS2-tagged 17S rRNA. Virtually no mature MS2-tagged 16S rRNA containing the J5/6 mutations was detectable above the background in any of the gradient fractions, demonstrating that these mutations impair 30S assembly and prevent normal maturation of the 16S 5′ end by RNase G. Heterogeneous primer extension products may reflect inaccurate processing of the triple mutant pre-rRNA (Figure 3E). We obtained similar results for the G107U single mutation and the A59C, A60C double mutation (Supplementary Figure S3), although ~2% of G107U MS2–16S rRNA was able to form 70S ribosomes. Therefore, even a single base change in the J5/6 motif severely impairs 30S biogenesis in *E. coli*.

J5/6 mutations locally perturb the rRNA structure

To determine if the J5/6 mutations prevent the 16S 5′ domain from folding normally, we probed the secondary structure of the 5′ domain rRNA using SHAPE chemical footprinting. SHAPE chemical footprinting is sensitive to the flexibility of the RNA backbone and the conforma-
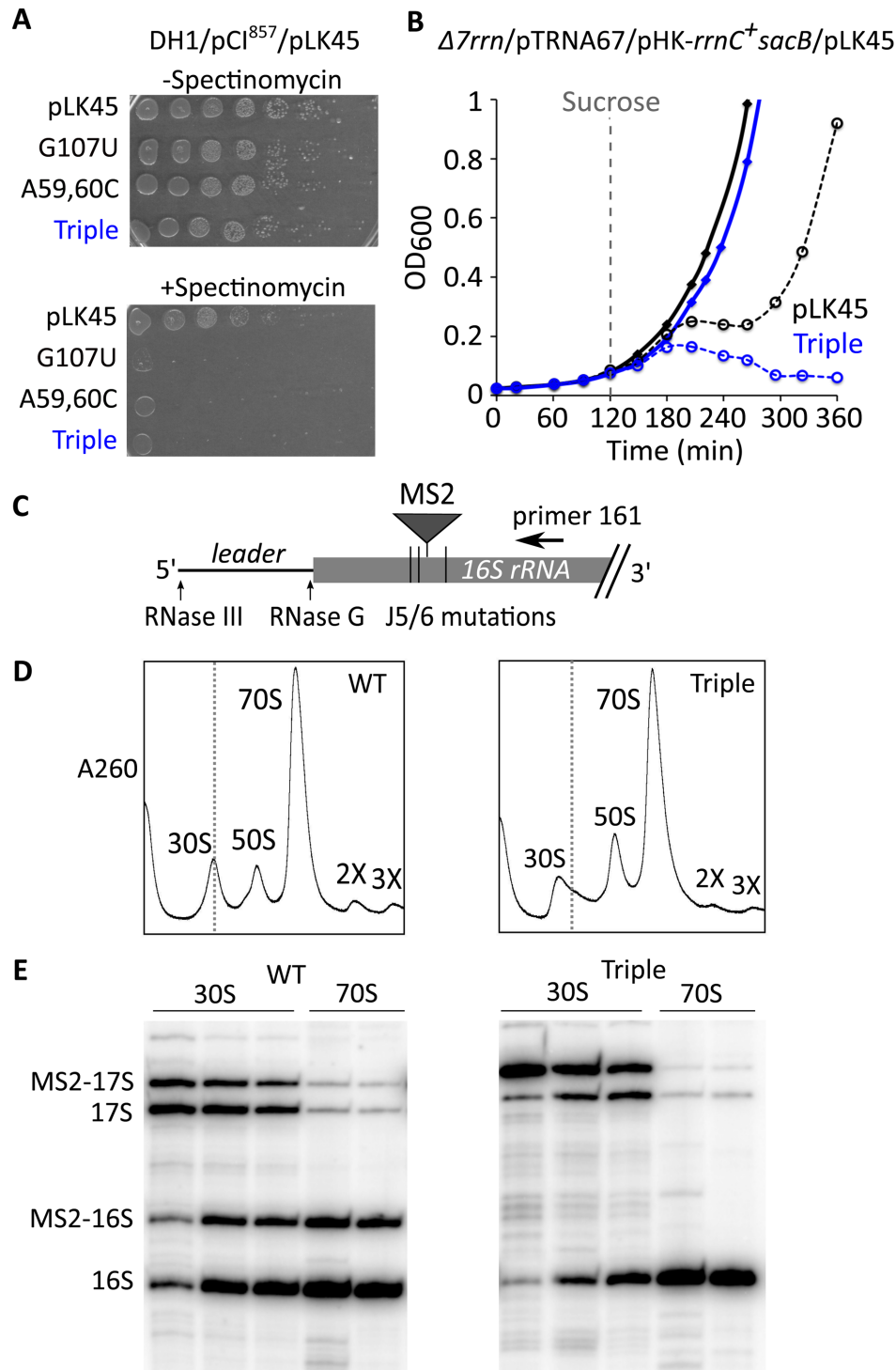
Figure 3. Mutations in J5/6 are recessive lethal and inhibit 30S assembly and maturation. (**A**) Growth of DH1/ pCI[857] cells transformed with pLK45 or derivatives containing J5/6 mutations in Figure 1A (middle). Ten-fold serial dilutions were spotted on LB agar with or without 10 μg/ml spectinomycin at 42°C (pLK45 expressed). (**B**) Growth of Δ7rrn/pTRNA67/pHK-*rrnC*+*sacB*/pLK45 (black) or Δ7rrn/pTRNA67/pHK-*rrnC*+*sacB*/pLK45-Triple (blue) at 37°C. Cultures were continued (solid lines), or 3% sucrose was added after 120 min to select for loss of the *rrnC* helper plasmid (dashed lines). (**C**) Plasmid-encoded rRNA is marked with an MS2 hairpin (triangle) in 16S h6. The relative locations of J5/6 mutations, processing sites for RNase III (17S rRNA) and RNase G (mature 16S 5′ end), and the priming site for cDNA synthesis in panel E, are indicated. (**D**) Sucrose gradient profiles from MRE600 transformed with pSpur (WT, left panel) and pSpur-Triple (J5/6 Triple mutant, right panel). See Supplementary Figure S3A for G107U and double mutants. The 30S peak is broad and light when cells express J5/6 mutant 16S rRNA, suggesting many particles are incompletely assembled. The dotted gray line indicates the sedimentation of mature 30S complexes. (**E**) Primer extension to map the 5′ end of 16S rRNA extracted from peak fractions of the sucrose gradient in (D). The MS2 hairpin in h6 creates longer primer extension products, distinguishing pSpur-encoded MS2-tagged rRNA from chromosomally encoded rRNA. Products corresponding to mature (16S) and immature (17S) rRNA are indicated. See Supplementary Figure S3B for bar graph of each rRNA species (*n* ≥ 2). The J5/6 mutant pre-rRNA is not processed to MS2–16S and does not enter the 70S fraction.

tion of the 2′ OH group (41), which can be influenced by nearby proteins (42). With some exceptions, such as 16S h12, which requires bS16 to adopt the native secondary structure (14,43), and J5/6 itself, the SHAPE data for both the WT and J5/6 mutant rRNAs were consistent with the known secondary structure of the 16S 5′ domain (Supplementary Figure S4A). Although the addition of ribosomal proteins uS4, uS17, bS20 and bS16 that bind the 5′ domain stabilized the RNA overall, the J5/6 mutations increased the reactivity of h13, the J4/5 junction and an internal loop in 16S h17 that forms part of the bS16 interaction site (red dots in h17 in Supplementary Figure S4B). In contrast, 16S h15, the four-way junction between h8-h10 that binds bS20, and interactions between h16 and h18 that bind uS4, were more folded in the triple J5/6 mutant than in the WT RNA (blue dots in Supplementary Figure S4B). These changes in SHAPE modification suggested that the J5/6 mutations prevent native packing between h17 and h15 against h5, thereby trapping the 5′ domain in an unproductive conformation. As discussed below, these differences in SHAPE reactivity are consistent with stabilization of a non-native 5′ domain assembly intermediate by the J5/6 mutations.

J5/6 mutations stabilize an assembly intermediate

Previous hydroxyl radical footprinting (15) and single molecule FRET experiments (18) showed that assembly of the 16S 5′ domain passes through an intermediate in which h3 is flipped away from the rest of the domain and from protein uS4 (Figure 4A). Protein uS4 binds the 5′ domain RNA when h3 is in either its flipped (F) or native (N) conformations (18). The equilibrium between these conformations of h3 was measured by ensemble fluorescence experiments, in which 5′ domain RNA with Cy3 attached near the end of h3 was titrated with Cy5-labeled S4 protein. The increase in FRET efficiency with uS4 concentration (Figure 4B) was fit to an equation for the four state binding model in Figure 4A, yielding the equilibrium constant K_2 between the flipped (low FRET) and native (high FRET) uS4-RNA complexes (19).

Although the G107U and triple J5/6 mutations did not change the overall affinity of uS4, these mutations shifted the conformational equilibrium toward the flipped intermediate complex, relative to uS4 complexes with the WT 5′ domain (compare black and blue plateaus in Figure 4B and left bars in Figure 4C). The addition of proteins bS16 and bS20 to the complex stabilized the native conformation of h3 in the S4 binding site, as previously observed (19). Nevertheless, even bS16 and bS20 could not fully overcome the preference of J5/6 mutants for the flipped intermediate conformation of h3, compared to the WT 5′ domain (right bars in Figure 4C).

Because the N-terminus of protein bS20 directly interacts with J5/6, and because bS20 also increases the stable addition of bS16 during 30S assembly (16,17), we compared binding of S20 to WT and J5/6 mutant RNAs by native PAGE (Supplementary Figure S5). The K_D for the WT 5′ domain RNA was ≤ 15 nM bS20, whereas it was above 30 nM bS20 for the G107U or triple J5/6 mutant RNA (Supplementary Figure S5B). This difference was not substantially rescued by the presence of uS4 (Supplementary Figure S5B).
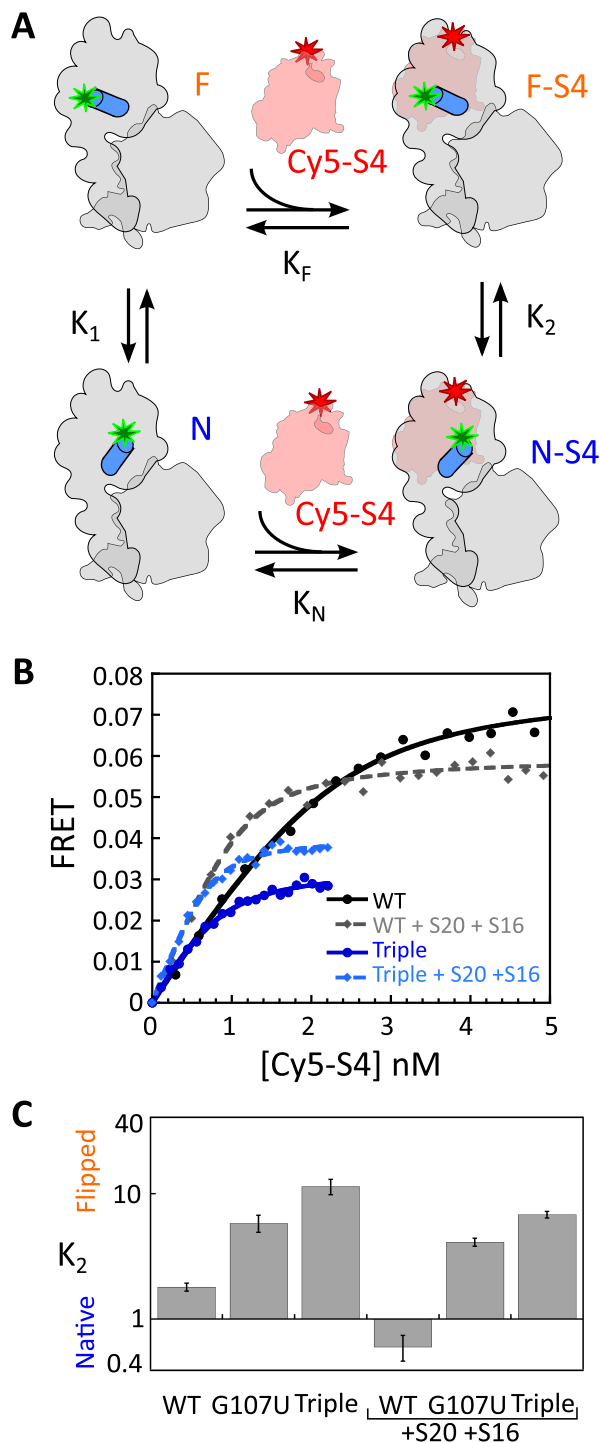

Figure 4. Conformation of 16S helix 3 by FRET. (**A**) Four-state model for protein uS4 (pink) binding to the 5′ domain of the 16S rRNA. 16S h3 (blue cylinder) can adopt either a native (N) high FRET or flipped (F) low FRET conformation. This equilibrium constant, K_2, can be determined from the FRET efficiency of the complexes. (**B**) Titration of 0.2 nM Cy3-labeled RNA with Cy5-S4 protein. The 16S 5′ domain was extended and hybridized with Cy3-SA5 oligomer. A higher FRET endpoint reflects a larger proportion of native uS4 complexes. Data were fit to a quadratic binding model (see Materials and Methods) to obtain K_2. Circles and smooth line, Cy5-S4 only; diamonds and dashed line, Cy5-S4 plus bS16 and bS20. (**C**) Equilibrium between native (N•S4) and flipped (F•S4) complexes, K_2, with and without bS16 and bS20. Single and triple J5/6 mutations raise the proportion of flipped complexes.

S5C). Thus, the J5/6 mutations weaken the bS20–5′domain interactions. This suggests a specific folding defect that prevents restructuring of the J5/6 junction.

Altogether, the results of the SHAPE footprinting, uS4 and bS20 binding assays show that the J5/6 mutations favor a 5′ domain assembly intermediate, and disfavor native-like complexes in which 16S h3 is docked against protein S4. The J5/6 mutations could exert this effect either by directly weakening interactions between J5/6 and surrounding elements such as the N-terminal helix of bS20, or by preventing the formation of an early metastable structure that facilitates later refolding of h3. Because h3 is directly connected to h1 at the 5′ end of the 16S rRNA and to the central pseudoknot which links the 16S 5′, central and 3′ domains in the mature 30S ribosome, misdocking of h3 has the potential to inhibit later stages of 30S assembly, thereby explaining why the J5/6 mutations block 5′ processing of the 16S rRNA in *E. coli*.

J5/6 triple mutation causes incomplete assembly of 30S 3′ domain

To gain greater insight into how the J5/6 region affects 30S ribosome biogenesis overall, we probed the structure of the 16S 3′ domain (30S head) by X-ray hydroxyl radical footprinting. *In vivo* hydroxyl radical footprinting is a powerful method for determining the solvent accessibility of the RNA backbone of even heterogeneous and difficult-to-isolate species (44). We exposed MRE600 *E. coli* cells transformed with the pSpur and pSpur-Triple plasmids to a synchrotron X-ray beam, which generates hydroxyl radical in the cytoplasm. Extension of a primer covering the spectinomycin resistance point mutation 16S 1193U was used to selectively analyze the footprinting pattern of the 3′ domain of plasmid-encoded 16S rRNA. The 16S 3′ domain is one of the last regions of the 30S ribosome to assemble and is bound by tertiary assembly proteins uS3 and uS2 (16,45). In order to identify structural differences in the triple mutant pre-30S ribosomes, hydroxyl radical cleavage of pSpur and pSpur-Triple encoded rRNAs were compared to each other and to unirradiated controls (Figure 5A). Nucleotides with at least a 50% change in the solvent accessibility in the triple mutant versus the pSpur control (Figure 5B) were mapped onto the 16S secondary structure and the tertiary structure of the 16S rRNA in the 30S ribosome (Figure 5C and D).

In the region covered by our primer extension assay, h35-h37 and h2, which form the 'neck' of the 30S ribosome, were strongly perturbed by the J5/6 mutations. Helix 36 extends down the solvent side of the 30S ribosome and interacts with the minor groove of nt 16–19 that form the central pseudoknot. Helix 36 also packs against h25, forming the binding site for protein uS2. These nucleotides were more exposed in the J5/6 mutant, suggesting that this region is unfolded and not recognized by protein uS2. Milder perturbations in h33 and h34 lie under the recognition site for protein uS3. Exposure of the h2, h33 and h36 has been observed in other *in vivo* probing experiments of immature ribosomes (44,46), suggesting a common barrier or 'checkpoint' to 30S maturation.

Central pseudoknot is not formed in J5/6 Triple mutant ribosomes

Formation of the central pseudoknot and binding of protein uS2 are among the final events in the 30S ribosome assembly (16,44,45,47,48). The partial folding of the 3′ domain in our *in vivo* footprinting results motivated us to examine whether the mutation in J5/6 has an impact on formation of the central pseudoknot. Allele-specific primer extension showed that residue A918 of the central pseudoknot is cleaved in ∼39% of non-irradiated BW25113/Triple mutant ribosomes (Figure 6A, left panel), suggesting that incomplete folding may leave this region accessible to nucleases, as reported previously (35). RimP, a non-enzymatic chaperone of 30S biogenesis, interacts with the 16S rRNA near the central pseudoknot. Deletion of *rimP* results in decreased stability of the central pseudoknot and depletion of proteins uS5 and uS12 from the 30S particles purified from the *ΔrimP* strain. Therefore, we tested whether overexpression of RimP could reduce cleavage of A918 in the triple mutant, and found that it did. Induction of RimP reduced the cleavage of the central pseudoknot at A918 from 31% to 19% (Figure 6A, right panel).

We further assayed the defect in central pseudoknot formation by testing whether this region is accessible to RNase H cleavage in the presence of an anti-central pseudoknot (anti-CP) oligomer (35). MS2–16S rRNA containing the J5/6 Triple mutation displayed two RNase H cleavage products in Figure 6B (lanes 3 and 4) whereas the WT rRNA was not cleaved (Figure 6B, lanes 9 & 10), suggesting that the central pseudoknot and hence the decoding active site is not formed in the Triple mutant. Perturbation of the central pseudoknot appears to be a hallmark of stalled biogenesis that prevents 30S maturation (35).

Mass spectrometry and electron microscopy of J5/6 Triple mutant

To more precisely pinpoint the stage of assembly that is blocked by the J5/6 mutations, we used quantitative mass spectrometry to determine which ribosomal proteins were missing in the J5/6 triple mutant pre-30S complexes. MS2 hairpin-tagged ribosomes with a wild type or triple mutant J5/6 sequence were purified by affinity with MS2 coat protein, which recovers all of the 30S proteins (Figure 7A). The total protein content of the complexes was analyzed using LC-MS/MS with excellent coverage of ribosomal proteins (Supplementary Figure S6), and the concentration of each protein was normalized to that of uS4 (Figure 7B). The immature triple mutant pre-30S complex lacked tertiary assembly proteins uS2 (∼70% reduction) and bS21 (∼99% reduction), which are commonly missing in pre-30S particles (35,44). This is consistent with *in vivo* footprinting results showing that the uS2 binding site is exposed to solvent. Partial depletion of uS3 further indicated that the head was not well formed.

Less expected was that the mutant pre-30S complexes entirely lacked uS12 and had a ∼50% abundance of uS5. The other 5′ domain proteins, uS4, bS16, uS17 and bS20, were present at normal levels. Thus, proteins bS16 and bS20 that bind near the J5/6 mutation still joined the complex, but proteins uS12 and uS5 that bind at the interface between the
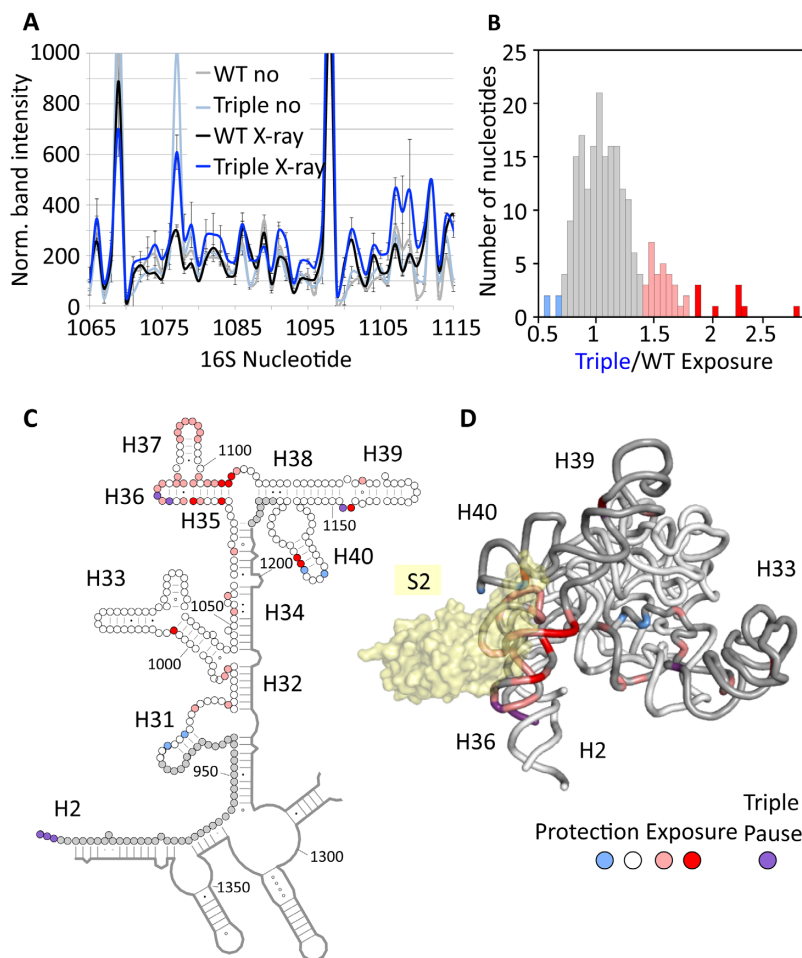
Figure 5. Incomplete assembly of 16S 3′ domain revealed by *in vivo* X-ray footprinting. (**A**) X-ray hydroxyl radical footprinting data for the 16S nt 1065–1115 (h35-h37) using a primer specific for the plasmid-borne spc^R allele. Average adjusted reactivity for each nucleotide, which correlates with relative exposure of the rRNA backbone (see Methods). Error bars, S.D. between three technical replicates. Black, pSpur-WT; blue, pSpur-Triple. Light colors, no X-ray exposure. (**B**) Histogram of relative backbone exposure for Triple mutant and WT 16S rRNA. Ratios 1.4–1.8 (pink) and >1.8 (red), nucleotides that are more exposed in pSpur-Triple ribosomes; ratios < 0.75 (blue), nucleotides that are more protected in pSpur-Triple ribosomes. (**C**) Nucleotides with altered backbone exposure mapped onto the 16S 3′ major domain. Colored as in (B). Purple residues exhibit a strong RT pause in pSpur-Triple RNA. Light grey residues were not detected by the allele-specific primer. (**D**) Three-dimensional structure of the 16S 3′ domain in the ribosome (solvent side) colored as in C with protein uS2 in yellow.

5′, central and 3′ domains were completely or partially prevented from binding. The absence of these proteins is consistent with the exposure of the central pseudoknot, which connects the three major domains of the 30S ribosome. Protein uS12 interacts with 16S h3 near the central pseudoknot, and failure to properly dock h3 could hinder binding of uS12. Protein uS5 directly interacts with the central pseudoknot as well as with protein uS4 and uS12 (49,50). Thus, we reasoned that defective recruitment of uS12 to the interface with the 5′ domain resulted in long-range perturbations in the 3′ domain 'neck' and head, preventing binding of protein uS2.

Since the *in vivo* footprinting and mass spectrometry results indicated specific defects in the interactions between the major domains of the 16S rRNA, we were motivated to visualize the overall structure of J5/6 mutant ribosomes. Negative stain electron micrograph images in Figure 7C suggest that structure of triple mutant 30S ribosome is severely distorted and heterogeneous, compared to wild

type MS2-tagged 30S ribosomes. For the WT 30S ribosomes, we observed the well-formed body, platform and head, as expected. Whereas, in the J5/6 triple mutant complexes, none of the normal connections between domains could be identified. This global collapse of the overall structure is reminiscent of pre-30S particles from a strain lacking RimP (35), an assembly factor that aids formation of the central pseudoknot and recruitment of uS5 (35,44,51), further suggesting a specific defect in inter-domain interactions.

DISCUSSION

Non-coding RNAs contain recurring sequence motifs that usually adopt similar three-dimensional structures in different contexts (7). Here, we describe a right angle (RA) motif at J5/6 that is conserved among SSU rRNAs (Supplementary Figure S1), yet is splayed apart in the mature ribosome (Figure 1, Supplementary Figure S2), suggesting it could
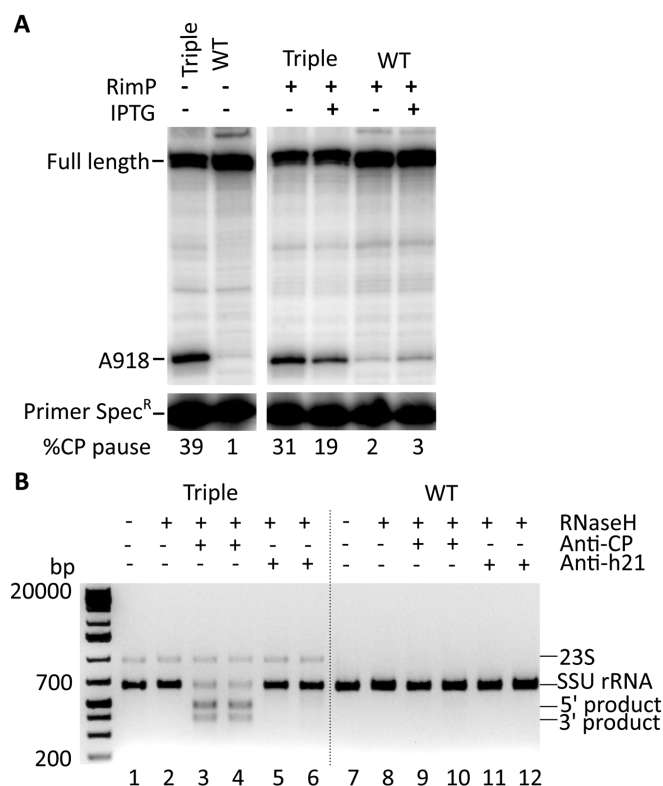
A

| RimP | - | - | + | + | + | + |
| IPTG | - | - | - | + | - | + |

Full length—

A918—

Primer Spec^R—

%CP pause 39 1 31 19 2 3

B

Figure 6. Formation of 16S central pseudoknot. (**A**) Allele-specific primer extension of spc^R plasmid-derived rRNA extracted from BW25113 cells. BW25113 is the parent of Keio collection strains used for assembly factor over-expression. Hydrolysis of pSpur-Triple rRNA results in a significant RT pause at 16S A918, which is reduced by IPTG induction of RimP. Fraction of cDNA paused at A918 (% CP pause) is indicated below the image. The pause site was assigned based on footprinting experiments and sequencing ladders in Figure 5. Lower panel shows unextended primer at the bottom of the sequencing gel. (**B**) Accessibility of 16S central pseudoknot was probed by hybridization of an Anti-CP oligomer and cleavage by RNase H (see Materials and Methods). Anti-h21 is a control oligomer complementary to a sequence in helix 21. A small amount of 23S rRNA (50S) co-purified with pSpur-Triple rRNA (pre-30S) (see Materials and Methods). Left lane, DNA MW standards. 2% agarose gel was stained with ethidium bromide. Cleavage of CP region indicates that J5/6 mutations impair formation of the central pseudoknot.

form an early metastable structure that guides 30S ribosome assembly. The importance of this motif is reinforced by the observation that the most prevalent natural J5/6 sequences also form stable RA motifs (Figure 2).

Although the J5/6 lies far from the center of the ribosome, mutations that disrupt the RA fold between h5 and h6 completely block pre-16S rRNA processing and are recessive lethal in *E. coli*. Structural probes and electron microscopy show that these mutations impart massive structural deformities by blocking formation of the central pseudoknot and interactions between the 5′, central, and 3′ domains of the 16S rRNA. The deformities correlate with a failure to recruit protein uS12, which contacts the central pseudoknot and all of the major 16S domains. Our results show that the J5/6 mutations do not prevent binding of proteins bS16 and bS20 that directly contact J5/6. Instead, the impact of the J5/6 mutations is felt at a later stage of 30S assembly around the central pseudoknot and in the 3′ domain

where protein uS2 must bind. These observations raise the question of how mutations in the 'foot' of 30S ribosome are communicated to its 'head'.

That J5/6 mutations act at a distance and at a later time of assembly suggests an allosteric mechanism in which a conformational switch at J5/6 favors an RNA conformation that is competent for the addition of tertiary assembly proteins. We propose that J5/6 and other structural motifs within the 16S rRNA are linked through a 'spine' of RNA helices that runs through the center of the 30S ribosome (Figure 8A). The connectivity of this spine involves conserved elements of the 16S rRNA and can be traced through the structures of the ribosome, from the h6 spur through J5/6 to h15, h4 and h3 within the 5′ body of the ribosome. Helix 3 is in turn connected to h28 in the 3′ domain via h1 and the central pseudoknot (h2), and to the central domain through h19 and h27. We propose that this central spine of RNA connects conformational switches in distal regions of the 16S rRNA that signal the correct assembly of the 5′ and 3′ domains. By linking these events with formation of the mRNA decoding site and processing of the 17S pre-rRNA, this allosteric model may ensure the quality of ribosome biogenesis. It also explains why a mutation in the normally stable body of the 16S rRNA has a catastrophic effect on overall assembly.

The results of footprinting and FRET experiments indicate how the conformation of J5/6 is transmitted to other regions of the 16S rRNA. *In vitro* SHAPE experiments showed that the J5/6 mutations prevent bS16 from natively packing h17 and h15 against h5, trapping the 5′ domain in an unproductive conformation. Loose packing of h15 communicates its negative effect to h3 via h4, which we confirmed by detecting 16S h3 in its non-native flipped conformation in the J5/6 mutant RNA using FRET (Figure 4C). Three-color smFRET experiments showed that h3 normally fluctuates between its native docked and non-native flipped conformations, but after S16 binding, the native h3 conformation persists for longer periods (17). The results here indicate that the J5/6 RA motif is needed for the normal effect of bS16 on h3 docking.

Proper folding of 16S h3 against protein uS4 has been recently established as a 'check point' that guides 30S assembly (15,17,18). Protein uS12 contacts the opposite face of h3 from uS4, and poor h3 docking likely hinders uS12 recruitment. Moreover, the non-native conformation of h3 negatively influences refolding of h1, which can no longer participate in the central pseudoknot that connects the 5′, central and 3′domains. Our footprinting, mass spectrometry and electron microscopy results show that the J5/6 mutations in the 16S 5′ domain do indeed impair assembly of the 3′ major domain and prevent formation of the central pseudoknot. The absence of the central pseudoknot prevents normal interactions between the major rRNA domains and with h44, thereby preventing formation of the decoding site.

Exposure of the central pseudoknot and the absence of uS2 and uS3 are hallmarks of assembly that has stalled at the pre-30S stage (35,44). Although similar types of pre-30S complexes accumulate in the absence of assembly factors such as ΔrimM and ΔyjeQ (52) or ΔrbfA (44,53), many of these pre-30S particles convert into mature 30S ribosomes. By contrast, pre-30S complexes with J5/6 mutations never

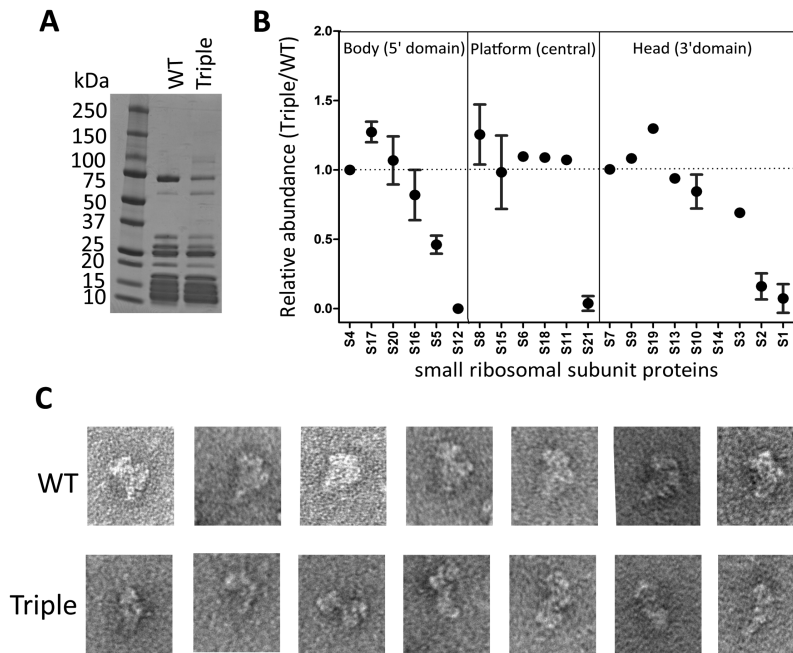**Figure 7.** Mass spectrometry and electron microscopy of isolated J5/6 Triple mutant ribosomes. (**A**) Profile of proteins from isolated MS2-tagged 30S ribosomes with WT and Triple mutant J5/6 sequence. 4–20% SDS PAGE with MW standards (left lane). (**B**) Relative abundance of r-proteins in Triple mutant 30S. Absolute concentration of each r-protein was quantified with high sequence coverage using LC MS/MS (~50% coverage for > 60% r-proteins, Supplementary Figure S6) and normalized to the amount of protein uS4 (see Materials and Methods). Error bars represent the standard deviation of two technical replicates. Peptides mapping to protein uS14 were not detected in this analysis. (**C**) Negative stain electron micrographs of WT and Triple mutant 30S complexes. The three-domain architecture of the mature 30S (body, head and platform) can be seen in WT complexes, whereas this global structure has collapsed in triple mutant complexes.
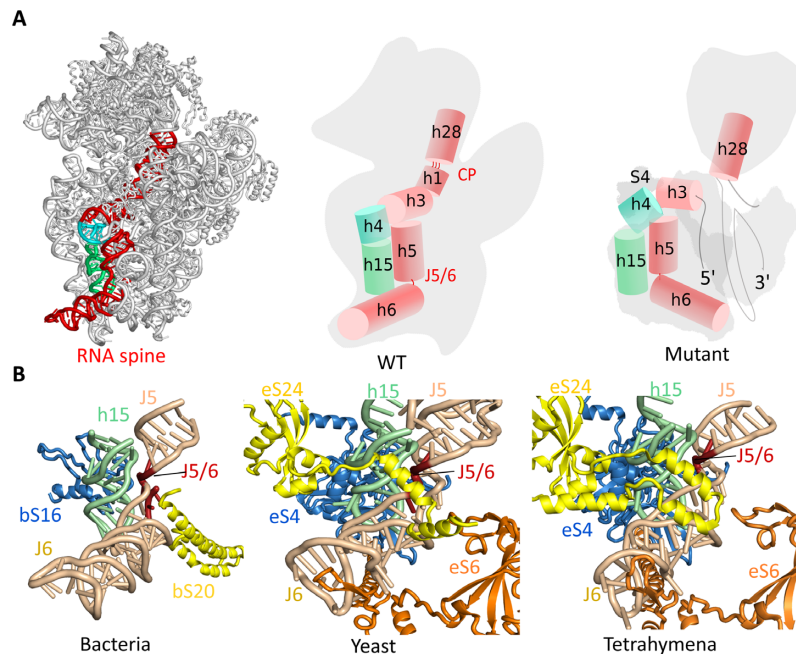

Figure 8. Allosteric communication of assembly status through an RNA spine. (**A**) A model depicting path of conformational switch originating from mutations in J5/6. Bacterial 30S showing RNA spine (left panel), helices and interactions that form the RNA spine (middle panel), mutation in J5/6 destabilizes the RNA spine that results in loss of interaction between 5′, central, and 3′ domain (right panel). (**B**) J5/6 motif is conserved across kingdoms. Bacterial 30S (2I2P), yeast 40S (5TGM; (57)) and *Tetrahymena* 40S (4V5O; (58)).

mature (Figure 3). This observation suggests that failure to correctly restructure certain 16S rRNA motifs, such as J5/6, raises the energy barrier for processing of the 17S pre-rRNA to a point where it is completely blocked (Figure 3, Supplementary Figure S3). Alternatively, continued assembly may cement an early rRNA folding error, committing the particle to a dead-end that cannot be easily reversed. Parallel assembly pathways (54) could bypass 16S misfolding in some cases (52). For example, ∼2% 16S rRNA containing the single J5/6 mutation G107U is processed and forms a 70S complex (Supplementary Figure S3). Individual complexes may stumble at different stages, explaining why we see heterogeneously deformed pre-30S particles in the negative stain electron micrographs of J5/6 mutant (Figure 7C).

The sequence between J5/6 encodes a conformational switch that is communicated to the three domains of 30S. Locating such a crucial switch in the 5′ domain is advantageous because early transcription and folding can guide proper assembly of rest of the ribosome. That the most prevalent J5/6 sequences form stable RA motifs within h5 and h6 suggests that the RA may act as a 'timer' to delay interactions with h15 until 5′ domain proteins are in place, although this motif may play some other role in stabilizing the folded SSU rRNA. A comparison of J5/6 in SSU from bacteria, yeast and *Tetrahymena* shows that its architecture and structural environment are conserved (Figure 8B). In bacterial ribosomes, J5/6 is sandwiched between bS16 and bS20 and packed against the tip of h15 that supplies the along-groove interactions with h5 that would normally be made by h6 in an RA fold. The 'splayed' conformation of J5/6 is stabilized by the N-terminal alpha helix of bS20. Interestingly, proteins eS4 and eS24 appear to fulfill similar roles in the yeast and *Tetrahymena* 40S ribosomes, in which an alpha helix from eS24 packs into open groove of J5/6. Thus, the structure of J5/6 is evolutionarily conserved and may serve a similar switch function during the biogenesis and assembly of eukaryotic 40S ribosomes (55).

SUPPLEMENTARY DATA

Supplementary Data are available at NAR Online.

ACKNOWLEDGEMENTS

FUNDING

REFERENCES

1. Noller,H.F. (1991) Ribosomal RNA and translation. *Annu. Rev. Biochem.*, **60**, 191–227.
2. Moore,P.B. and Steitz,T.A. (2005) The ribosome revealed. *Trends Biochem. Sci.*, **30**, 281–283.
3. Melnikov,S., Ben-Shem,A., Garreau de Loubresse,N., Jenner,L., Yusupova,G. and Yusupov,M. (2012) One core, two shells: bacterial and eukaryotic ribosomes. *Nat. Struct. Mol. Biol.*, **19**, 560–567.
4. Jaeger,L., Verzemnieks,E.J. and Geary,C. (2009) The UA˙handle: a versatile submotif in stable RNA architectures. *Nucleic Acids Res.*, **37**, 215–230.
5. Noller,H.F. (2005) RNA structure: reading the ribosome. *Science*, **309**, 1508–1514.
6. Stern,S., Weiser,B. and Noller,H.F. (1988) Model for the three-dimensional folding of 16 S ribosomal RNA. *J. Mol. Biol.*, **204**, 447–481.
7. Lescoute,A. and Westhof,E. (2006) Topology of three-way junctions in folded RNAs. *RNA*, **12**, 83–93.
8. Chworos,A., Severcan,I., Koyfman,A.Y., Weinkam,P., Oroudjev,E., Hansma,H.G. and Jaeger,L. (2004) Building programmable jigsaw puzzles with RNA. *Science*, **306**, 2068–2072.
9. Grabow,W.W., Zhuang,Z., Swank,Z.N., Shea,J.-E. and Jaeger,L. (2012) The right angle (RA) motif: a prevalent ribosomal RNA structural pattern found in Group I introns. *J. Mol. Biol.*, **424**, 54–67.
10. Grabow,W.W., Zhuang,Z., Shea,J.E. and Jaeger,L. (2013) The GA-minor submotif as a case study of RNA modularity, prediction, and design. *Wiley Interdiscip. Rev. RNA*, **4**, 181–203.
11. Gagnon,M.G. and Steinberg,S.V. (2002) GU receptors of double helices mediate tRNA movement in the ribosome. *RNA*, **8**, 873–877.
12. Adilakshmi,T., Ramaswamy,P. and Woodson,S.A. (2005) Protein-independent folding pathway of the 16S rRNA 5′ domain. *J. Mol. Biol.*, **351**, 508–519.
13. Dutca,L.M. and Culver,G.M. (2008) Assembly of the 5′ and 3′ minor domains of 16S ribosomal RNA as monitored by tethered probing from ribosomal protein S20. *J. Mol. Biol.*, **376**, 92–108.
14. Stern,S., Changchien,L.M., Craven,G.R. and Noller,H.F. (1988) Interaction of proteins S16, S17 and S20 with 16 S ribosomal RNA. *J. Mol. Biol.*, **200**, 291–299.
15. Ramaswamy,P. and Woodson,S.A. (2009) S16 throws a conformational switch during assembly of 30S 5′ domain. *Nat. Struct. Mol. Biol.*, **16**, 438–445.
16. Held,W.A., Ballou,B., Mizushima,S. and Nomura,M. (1974) Assembly mapping of 30 S ribosomal proteins from Escherichia coli. Further studies. *J. Biol. Chem.*, **249**, 3103–3111.
17. Abeysirigunawardena,S.C., Kim,H., Lai,J., Ragunathan,K., Rappé,M.C., Luthey-Schulten,Z., Ha,T. and Woodson,S.A. (2017) Evolution of protein-coupled RNA dynamics during hierarchical assembly of ribosomal complexes. *Nat. Commun.*, **8**, 492.
18. Kim,H., Abeysirigunawarden,S.C., Chen,K., Mayerle,M., Ragunathan,K., Luthey-Schulten,Z., Ha,T. and Woodson,S.A. (2014) Protein-guided RNA dynamics during early ribosome assembly. *Nature*, **506**, 334–338.
19. Abeysirigunawardena,S.C. and Woodson,S.A. (2015) Differential effects of ribosomal proteins and Mg $^{2+}$ ions on a conformational switch during 30S ribosome 5′-domain assembly. *RNA*, **21**, 1859–1865.
20. Paillart,J., Skripkin,E., Ehresmann,B., Ehresmann,C. and Marquet,R. (1996) A loop-loop "kissing" complex is the essential part of the dimer linkage of genomic HIV-1 RNA. *Proc. Natl. Acad. Sci. U.S.A.*, **93**, 5572–5577.
21. Zhang,F., Ramsay,E.S. and Woodson,S.A. (1995) In vivo facilitation of Tetrahymena group I intron splicing in Escherichia coli pre-ribosomal RNA. *RNA*, **1**, 284–292.
22. Powers,T. and Noller,H.F. (1990) Dominant lethal mutations in a conserved loop in 16S rRNA. *Proc. Natl. Acad. Sci. U.S.A.*, **87**, 1042–1046.
23. Youngman,E.M. and Green,R. (2005) Affinity purification of in vivo-assembled ribosomes for in vitro biochemical analysis. *Methods*, **36**, 305–312.
24. Asai,T., Zaporojets,D., Squires,C. and Squires,C.L. (1999) An Escherichia coli strain with all chromosomal rRNA operons inactivated: complete exchange of rRNA genes between bacteria. *Proc. Natl. Acad. Sci. U.S.A.*, **96**, 1971–1976.

25. Zaporojets,D., French,S. and Squires,C.L. (2003) Products transcribed from rearranged rrn genes of Escherichia coli can assemble to form functional ribosomes. *J. Bacteriol.*, **185**, 6921–6927.
26. Spedding,G. (1990) *Ribosomes and Protein Synthesis: A Practical Approach*. IRL Press at Oxford University Press.
27. Moazed,D., Van Stolk,B.J., Douthwaite,S. and Noller,H.F. (1986) Interconversion of active and inactive 30 S ribosomal subunits is accompanied by a conformational change in the decoding region of 16 S rRNA. *J. Mol. Biol.*, **191**, 483–493.
28. Jinks-Robertson,S., Gourse,R.L. and Nomura,M. (1983) Expression of rRNA and tRNA genes in Escherichia coli: evidence for feedback regulation by products of rRNA operons. *Cell*, **33**, 865–876.
29. Condon,C., French,S., Squires,C. and Squires,C.L. (1993) Depletion of functional ribosomal RNA operons in Escherichia coli causes increased expression of the remaining intact copies. *EMBO J.*, **12**, 4305–4315.
30. Mayerle,M., Bellur,D.L. and Woodson,S.A. (2011) Slow formation of stable complexes during coincubation of minimal rRNA and ribosomal protein S4. *J. Mol. Biol.*, **412**, 453–465.
31. Adilakshmi,T., Soper,S.F.C. and Woodson,S.A. (2009) Structural analysis of RNA in living cells by in vivo synchrotron X-ray footprinting. *Methods Enzymol.*, **468**, 239–258.
32. Das,R., Laederach,A., Pearlman,S.M., Herschlag,D. and Altman,R.B. (2005) SAFA: semi-automated footprinting analysis software for high-throughput quantification of nucleic acid footprinting experiments. *RNA*, **11**, 344–354.
33. Gupta,N. and Culver,G.M. (2014) Multiple in vivo pathways for Escherichia coli small ribosomal subunit assembly occur on one pre-rRNA. *Nat. Struct. Mol. Biol.*, **21**, 937–943.
34. Dator,R.P., Gaston,K.W. and Limbach,P.A. (2014) Multiple enzymatic digestions and ion mobility separation improve quantification of bacterial ribosomal proteins by data independent acquisition liquid chromatography—mass spectrometry. *Anal. Chem.*, **86**, 4264–4270.
35. Sashital,D.G., Greeman,C.A., Lyumkis,D., Potter,C.S., Carragher,B. and Williamson,J.R. (2014) A combined quantitative mass spectrometry and electron microscopy analysis of ribosomal 30S subunit assembly in E. coli. *Elife*, **3**, e04491.
36. Rames,M., Yu,Y. and Ren,G. (2014) Optimized negative staining: a high-throughput protocol for examining small and asymmetric protein structure by electron microscopy. *J. Vis. Exp.*, e51087.
37. Jaeger,L. and Leontis,N.B. (2000) Tecto-RNA: One-dimensional self-assembly through tertiary interactions. *Angew. Chem. Int. Ed.*, **39**, 2521–2524.
38. Ishikawa,J., Furuta,H. and Ikawa,Y. (2013) RNA Tectonics (tectoRNA) for RNA nanostructure design and its application in synthetic biology. *Wiley Interdiscip. Rev. RNA*, **4**, 651–664.
39. Grabow,W.W. and Jaeger,L. (2014) RNA self-assembly and RNA nanotechnology. *Acc. Chem. Res.*, **47**, 1871–1880.
40. Geary,C., Chworos,A., Verzemnieks,E., Voss,N.R. and Jaeger,L. (2017) Composing RNA Nanostructures from a Syntax of RNA Structural Modules. *Nano Lett.*, **17**, 7095–7101.
41. Steen,K.-A., Rice,G.M. and Weeks,K.M. (2012) Fingerprinting noncanonical and tertiary RNA structures by differential SHAPE reactivity. *J. Am. Chem. Soc.*, **134**, 13160–13163.
42. Peng,Y., Curtis,J.E., Fang,X. and Woodson,S.A. (2014) Structural model of an mRNA in complex with the bacterial chaperone Hfq. *Proc. Natl. Acad. Sci. U.S.A.*, **111**, 17134–17139.
43. Moazed,D., Stern,S. and Noller,H.F. (1986) Rapid chemical probing of conformation in 16 S ribosomal RNA and 30 S ribosomal subunits using primer extension. *J. Mol. Biol.*, **187**, 399–416.
44. Clatterbuck Soper,S.F., Dator,R.P., Limbach,P.A. and Woodson,S.A. (2013) In vivo X-ray footprinting of pre-30S ribosomes reveals chaperone-dependent remodeling of late assembly intermediates. *Mol. Cell*, **52**, 506–516.
45. Talkington,M.W.T., Siuzdak,G. and Williamson,J.R. (2005) An assembly landscape for the 30S ribosomal subunit. *Nature*, **438**, 628–632.
46. McGinnis,J.L., Liu,Q., Lavender,C.A., Devaraj,A., McClory,S.P., Fredrick,K. and Weeks,K.M. (2015) In-cell SHAPE reveals that free 30S ribosome subunits are in the inactive state. *Proc. Natl. Acad. Sci. U.S.A.*, **112**, 2425–2430.
47. Holmes,K.L. and Culver,G.M. (2004) Mapping structural differences between 30S ribosomal subunit assembly intermediates. *Nat. Struct. Mol. Biol.*, **11**, 179–186.
48. Powers,T., Daubresse,G. and Noller,H.F. (1993) Dynamics of in vitro assembly of 16 S rRNA into 30 S ribosomal subunits. *J. Mol. Biol.*, **232**, 362–374.
49. Xu,Z. and Culver,G.M. (2010) Differential assembly of 16S rRNA domains during 30S subunit formation. *RNA*, **16**, 1990–2001.
50. Nord,S., Bhatt,M.J., Tükenmez,H., Farabaugh,P.J. and Wikström,P.M. (2015) Mutations of ribosomal protein S5 suppress a defect in late-30S ribosomal subunit biogenesis caused by lack of the RbfA biogenesis factor. *RNA*, **21**, 1454–1468.
51. Bunner,A.E., Nord,S., Wikström,P.M. and Williamson,J.R. (2010) The effect of ribosome assembly cofactors on in vitro 30S subunit reconstitution. *J. Mol. Biol.*, **398**, 1–7.
52. Thurlow,B., Davis,J.H., Leong,V., F. Moraes,T., Williamson,J.R. and Ortega,J. (2016) Binding properties of YjeQ (RsgA), RbfA, RimM and Era to assembly intermediates of the 30S subunit. *Nucleic Acids Res.*, **44**, 9918–9932.
53. Inoue,K., Alsina,J., Chen,J. and Inouye,M. (2003) Suppression of defective ribosome assembly in a rbfA deletion mutant by overexpression of Era, an essential GTPase in Escherichia coli. *Mol. Microbiol.*, **48**, 1005–1016.
54. Mulder,A.M., Yoshioka,C., Beck,A.H., Bunner,A.E., Milligan,R.A., Potter,C.S., Carragher,B. and Williamson,J.R. (2010) Visualizing ribosome biogenesis: parallel assembly pathways for the 30S subunit. *Science*, **330**, 673–677.
55. Kressler,D., Hurt,E. and Baßler,J. (2017) A puzzle of life: crafting ribosomal subunits. *Trends Biochem. Sci.*, **42**, 640–654.
56. Berk,V., Zhang,W., Pai,R.D. and Cate,J.H.D. (2006) Structural basis for mRNA and tRNA positioning on the ribosome. *Proc. Natl. Acad. Sci. U.S.A.*, **103**, 15830–15834.
57. Melnikov,S., Mailliot,J., Rigger,L., Neuner,S., Shin,B., Yusupova,G., Dever,T.E., Micura,R. and Yusupov,M. (2016) Molecular insights into protein synthesis with proline residues. *EMBO Rep.*, **17**, 1776–1784.
58. Rabl,J., Leibundgut,M., Ataide,S.F., Haag,A. and Ban,N. (2011) Crystal structure of the eukaryotic 40S ribosomal subunit in complex with initiation factor 1. *Science*, **331**, 730–736.